Bioactive Materials 6 (2021) 375–385

Contents lists available at ScienceDirect

Bioactive Materials

journal homepage: http://www.keaipublishing.com/biomat

A novel mechanism of inhibiting in-stent restenosis with arsenic trioxide drug-eluting stent: Enhancing contractile phenotype of vascular smooth muscle cells via YAP pathway

Yinping Zhao[a,b], Guangchao Zang[a], Tieying Yin[b], Xiaoyi Ma[c], Lifeng Zhou[c], Lingjuan Wu[d], Richard Daniel[d], Yunbing Wang[e], Juhui Qiu[b,**], Guixue Wang[b,*]

[a] Laboratory of Tissue and Cell Biology, Lab Teaching & Management Center, Chongqing Medical University, Chongqing, 400016, China
[b] Key Laboratory for Biorheological Science and Technology of Ministry of Education, State and Local Joint Engineering Laboratory for Vascular Implants, Bioengineering College of Chongqing University, Chongqing, 400030, China
[c] Beijing Amsinomed Medical Co., Ltd, Beijing, 100021, China
[d] Medical School, Newcastle University, Newcastle Upon Tyne, NE2 4AX, UK
[e] National Engineering Research Center for Biomaterials, Sichuan University, Chengdu, 610065, China

ARTICLE INFO

Keywords:
Arsenic trioxide (ATO)
Bioactive
Yes-associated protein (YAP)
In-stent restenosis (ISR)

ABSTRACT

Objective: Arsenic trioxide (ATO or As_2O_3) has beneficial effects on suppressing neointimal hyperplasia and restenosis, but the mechanism is still unclear. The goal of this study is to further understand the mechanism of ATO's inhibitory effect on vascular smooth muscle cells (VSMCs).

Methods and results: Through *in vitro* cell culture and *in vivo* stent implanting into the carotid arteries of rabbit, a synthetic-to-contractile phenotypic transition was induced and the proliferation of VSMCs was inhibited by ATO. F-actin filaments were clustered and the elasticity modulus was increased within the phenotypic modulation of VSMCs induced by ATO *in vitro*. Meanwhile, Yes-associated protein (YAP) nuclear translocation was inhibited by ATO both *in vivo* and *in vitro*. It was found that ROCK inhibitor or YAP inactivator could partially mask the phenotype modulation of ATO on VSMCs.

Conclusions: The interaction of YAP with the ROCK pathway through ATO seems to mediate the contractile phenotype of VSMCs. This provides an indication of the clinical therapeutic mechanism for the beneficial bioactive effect of ATO-drug eluting stent (AES) on in-stent restenosis (ISR).

1. Introduction

As one of the oldest poisons, arsenic trioxide (ATO or As_2O_3) is also known to have a wonder drug effect for treating numerous malignant diseases, ranging from infections such as malaria, ulcers, bubonic plague and even cancers [1]. Interestingly, its use has been documented for the treatments of various ailments in China as early as 2, 400 years ago [2]. Until to 1995, ATO was identified as the active component of traditional Chinese medicine called “Ai-Ling #1” [3,4] and approved by US FDA (Food and Drug Administration) for treating patients with acute promyelocytic leukemia (APL) [5,6]. ATO has also shown efficacy against other tumors largely due to its anti-proliferative or pro-apoptotic properties [7], and because of this anti-proliferative effect, ATO was introduced into the field of drug-eluting stents (DES) [8,9]. Our previous data proved that ATO-drug eluting stent (AES) has the capacity to both promote rapid re-endothelialization and inhibit in-stent restenosis (ISR) in the responding concentration of ATO [10], but the mechanisms by which ATO inhibits ISR are largely unknown.

Vascular smooth muscle cells (VSMCs) are the fundamental cellular components, and primarily govern structural integrity and regulate vascular tone, of the blood vessel wall. Unlike many terminally differentiated cells, VSMCs possess remarkable plasticity [11]. In response to environmental stimuli, such as injury or stent implantation, VSMCs can go through dramatic phenotypic transitions from a differentiated (‘contractile’) phenotype to a dedifferentiated (‘synthetic’) phenotype [12] exhibiting different function and morphology phenotypes [13]. It is well established that the synthetic phenotype of VSMCs is the cause of vascular proliferation remodeling diseases such as hypertension [14],

Peer review under responsibility of KeAi Communications Co., Ltd.
* Corresponding author.
** Corresponding author.
E-mail addresses: jhqiu@cqu.edu.cn (J. Qiu), wanggx@cqu.edu.cn (G. Wang).

https://doi.org/10.1016/j.bioactmat.2020.08.018
Received 9 May 2020; Received in revised form 13 August 2020; Accepted 23 August 2020

atherosclerosis [15], intimal hyperplasia and ISR [10,16,17]. Therefore, the effective regulation of VSMCs phenotype modulation is crucial for the treatment of cardiovascular diseases and regeneration. To the best of our knowledge, the effect of ATO on VSMCs phenotype modulation in ISR has not been investigated.

Yes-associated protein (YAP) is a key co-transcription factor in the Hippo signaling that plays an important role in vascular remodeling and can regulate VSMCs phenotype transition [18]. Generally, YAP induces VSMCs synthetic phenotype and promotes neointima formation through inhibiting smooth muscle-specific gene expression while promoting smooth muscle proliferation and migration *in vitro* and *in vivo* [19,20]. So, blocking the induction of YAP would be a potential therapeutic approach for ameliorating vascular occlusive diseases. Based on the aforementioned findings, we speculated that the ISR inhibiting drug ATO could promote VSMCs contractile phenotype transition through inhibition of YAP activity.

In this study, we demonstrate that ATO can increase the elastic modulus via F-actin assembly and induce a synthetic-to-contractile phenotypic transition of VSMCs *in vivo*, through stent implantation or *in vitro*, in cell culture model. The negative role of YAP in mediating ATO regulation of VSMC phenotypic modulation is also identified.

2. Materials and methods

2.1. Materials

316LVM stents (2.0 × 13 mm, diameter × length), have the strut width of 0.13 mm and the strut thickness of 0.12 mm. The clinical grade ATO-drug eluting stent (AES) was prepared by coating the bare metal stent (BMS) with a high molecular polymer of poly-L-lactic acid (PLLA) and As_2O_3 (3 μg/mm). In brief, 1% (w/w) solution of PLLA in tetrahydrofuran with or without As_2O_3 was sprayed onto the stent wires to form polymer coating-metal stent (PMS) and AES. Each coated stent contained ~0.1 mg of PLLA plus 40 μg of As_2O_3. The thickness of the polymer layer on the wire ranged from 6 to 10 μm (mean 8 μm). After spraying, the coating stents shall be dried for more than 48 h to make the tetrafluoroethylene volatilize to reach the specified residual standard. All the above stents were prepared and provided by Beijing Amsinomed Medical Company.

2.2. Animals implantations

The Guide for Chinese Animal Care and Use Committee standards was followed for the animal housing and surgical procedures. All *in vivo* procedures were done in accordance with protocols approved by the Animal Ethics Committee of Chongqing University. New Zealand male rabbits, weighing 2.5–3.5 kg/each, were obtained from and housed in the Experimental Animal Center of Daping hospital (Chongqing, China). The rabbits were randomly divided into three groups, i.e., BMS, PMS, and AES, and the analysis was repeat 3 times. The implantation of stents into New Zealand male rabbits was performed as described previously [10].

2.3. Hematoxylin and eosin (HE) staining and immunocytochemistry

HE staining was performed by Servicebio company (Wuhan, China). For immunocytochemistry, stented arterial segments were fixed in 4% paraformaldehyde, permeabilized (PBS with 0.1% triton X-100), blocked (1% bovine serum albumin (BSA)/0.01% triton X-100), and incubated with one of the following antibodies: mouse anti-human α-SMA and rabbit anti-human osteopontin (OPN, 1:50; 4 °C overnight; Serotec, Raleigh, NC, USA), diluted in blocking buffer. Subsequently, the samples were incubated with Alexa Fluor 488 or 594-conjugated goat anti-mouse or goat anti-rabbit antibodies (1:100; 1 h at RT; Invitrogen) and counter-stained with Hoechst nuclear dye (1:400 in PBS; 10 min; Sigma).

2.4. Cell culture

Human aortic SMC lines (HASMC) and rat SMC lines (A7r5) were cultured in DMEM (Gibco; #11885-092) supplemented with 10% fetal bovine serum, 100 U/mL penicillin and 100 μg/mL streptomycin at 37 °C in humidified atmosphere containing 5% CO_2. Primary porcine coronary artery smooth muscle cells (PCASMCs) were isolated from porcine coronary artery as previously reported [21,22], identified by α-SMA (ab7817, Abcam, 1:1000) staining, and cultured in smooth muscle cell medium (SMCM, Sciencell; #1101) supplemented low fetal bovine serum with 5%, and high fetal bovine serum with 20%. PCASMC passages 4 to 10 were sed for all experiments.

2.5. Cell viability of VSMCs in vitro

The viability of VSMCs at different concentration of ATO (0, 2, 4, 6, 8, and 10 μM or 0, 2, 4 and 6 μM) *in vitro* were performed through 3-(4,5-dimethylthiazol-2-yl)-5-(3-carboxymethoxyphenyl)-2-(4-sulfophenyl)-2H-tetrazolium, inner salt (MTS assay) by a CellTiter 96®AQueous One Solution Reagent (Promega, China) according to the manufacturer's instructions. The optical absorption density was measured at 490 nm using a microplate reader (Biotek ELx800, US).

2.6. Western blot (WB) assay, immunofluorescence staining (IF) and flow cytometry

WB analysis was carried out as previously reported [23]. Whole cell lysate samples were prepared using the RIPA buffer (Thermo Fisher Scientific) supplemented with a protease inhibitor mixture. Antibodies against GAPDH (D16H11, 5174, Cell Signaling Technology, 1:3000), α-SMA (ab7817, Abcam, 1:1000), SM22α (ab14106, Abcam, 1:1000), Osteopontin (ab8848, Abcam, 1:1000), YAP (D8H1X, 14074, Cell signal technology, 1:1000) and p-YAP (ab62751, Abcam, 1:1000) were used to determine the abundance of individual proteins.

IF was performed according to a method described previous [10]. The following primary antibodies against α-SMA (ab7817, Abcam, 1:300), SM22α (ab14106, Abcam, 1:300), Calponin (bs-0095R, Bioss, 1:250), YAP (D8H1X, 14074, Cell signal technology, 1:300), p-YAP (ab62751, Abcam, 1:300), and phalloidin (Proteintech, 1:200) were used. Nucleus stained with DAPI (Boster Institute of Biotechnology, Wuhan, China). The images were acquired with a laser scanning confocal microscope (Leica SP8, Germany).

Mitochondrial membrane potential staining by JC-1 Assay Kit (Beyotime, China) was detected by flow cytometry. In brief, the VSMCs (A7r5 and PCASMCs) were seeded in 6-well plates and incubated for 2 d. ATO treatment lasted for 1 d. The cells were washed with PBS solution and then mixed with 1 mL JC-1 working fluid. The cells were then incubated at 37 °C for 30 min. After incubation, the supernatant was removed and the chondrocytes were washed twice with JC-1 staining buffer. Subsequently, 0.25% trypsinase was used to obtain a cell suspension which was centrifuged and subsequently suspended in phosphate buffered saline (PBS) and filtered through 40 mm nylon cell strainer. The mitochondrial membrane potential was then measured using FACS Calibur (BD Biosciences, CA, USA).

2.7. RNA preparation for sequencing

Total RNA was extracted using TRIzol Reagent (Takara) according to the manufacturer's instructions. The concentration, quality and integrity were determined using a NanoDrop spectrophotometer (Thermo Scientific). Finally, eight samples (SS0, SS2, SH0 and SH2, 2 replicates) were used for libraries construction. A total amount of 3 μg RNA per sample was used as input material for the RNA sample preparations. Sequencing libraries were generated using NEBNext® Ultra™ RNA Library Prep Kit for Illumina® (NEB, USA) following manufacturer's recommendations and index codes were added to attribute sequences to

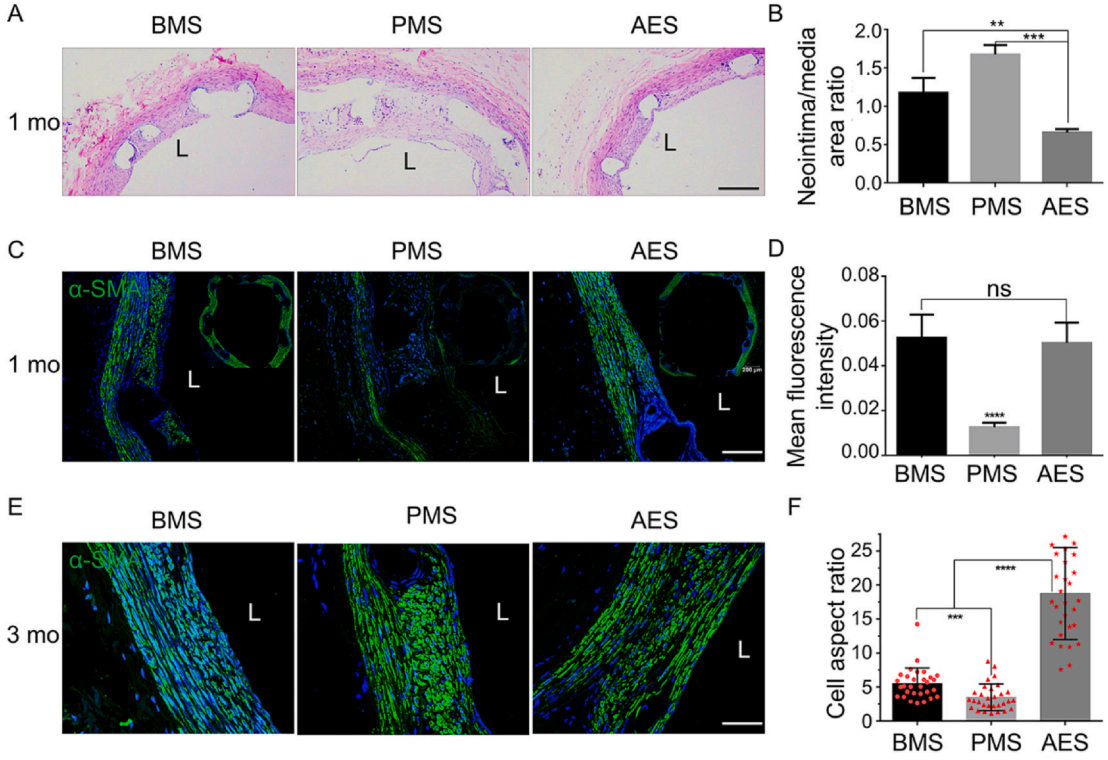

Fig. 1. *In vivo*, AES inhibits in-stent restenosis and induces differentiation of smooth muscle cells in neointima. (A) Hematoxylin and eosin (HE) staining of vascular after stent implantation for 1 mo, scar bar = 200 μm. (B) The statistical results of neointima/media area ratio for HE staining after stent implantation for 1 mo, n = 3. (C) Immunofluorescent staining with α-SMA (green) after stent implantation for 1 mo, scar bar = 100 μm. (D) The statistical results of mean fluorescence intensity of α-SMA after stent implantation for 1 mo in neointima, n = 6. (E) Immunofluorescent staining with α-SMA (green) after stent implantation for and 3 mo, scar bar = 50 μm. (F) The statistical results of cell aspect ratio (cell long/short axis ratio) of VSMCs after stent implantation for 3 mo in neointima, n = 30. "L" for the lumen. BMS (bare metal stent), PMS (polymer coating-metal stent), and AES (arsenic trioxide-drug eluting stent); 1 mo (1 month) and 3 mo (3 months), "ns" means no significance, and *P* values < 0.01 (**), < 0.001 (***) and < 0.0001 (****).

each sample. Briefly, mRNA was purified from total RNA using poly-T oligo-attached magnetic beads. Fragmentation was carried out using divalent cations under elevated temperature in NEBNext First Strand Synthesis Reaction Buffer (5X). First strand cDNA was synthesized using random hexamer primer and M-MuLV Reverse Transcriptase (RNase H^-). Second strand cDNA synthesis was subsequently performed using DNA Polymerase I and RNase H. Remaining overhangs were converted into blunt ends via exonuclease/polymerase activities. After adenylation of 3′ ends of DNA fragments, NEBNext Adaptor with hairpin loop structure were ligated to prepare for hybridization. In order to select cDNA fragments of preferentially 150–200 bp in length, the library fragments were purified with AMPure XP system (Beckman Coulter, Beverly, USA). Then 3 μL USER Enzyme (NEB, USA) was used with size-selected, adaptor-ligated cDNA at 37 °C for 15 min followed by 5 min at 95 °C before PCR. Then PCR was performed with Phusion High-Fidelity DNA polymerase, Universal PCR primers and Index (X) Primer. At last, PCR products were purified (AMPure XP system) and library quality was assessed on the Agilent Bioanalyzer 2100 system. RNA library construction and sequencing were performed by Novogene Co., LTD.

2.8. Differential expression analysis

Differential expression analysis of two conditions/groups (two biological replicates per condition) was performed using the DESeq R package (1.18.0). Gene Ontology (GO) enrichment analysis of differentially expressed genes was implemented by the GOseq R package, in which gene length bias was corrected. GO terms with corrected *P*-value less than 0.05 were considered significantly enriched by differential expressed genes.

2.9. Quantitative real-time PCR (qPCR) validation of differentially expressed genes and signaling pathway genes

Total RNA was extracted using the TRIzol Reagent (Takara), according to the manufacturer's instructions. The housekeeping gene GAPDH was used as a reference control to normalize the expression level. We performed qPCR using a CXF96 system (Bio-rad, USA). The primer sequences were:

YAP (forward: 5′- TCGGCAGGCAATACGGAATA-3'; reverse: 5′-CAT GCTGAG GCCACTGTCTGT-3′), α-SMA (forward: 5′-CAGGGAGTGATG GTTGGAAT-3'; reverse: 5′-GGTGATGATGCCGTGTTCTA-3′), Calponin (forward: 5′-ATG GGCACCAATAAGTTTGC-3'; reverse: 5′-GACCTGGCT CAAAGATCTGC-3′), RhoA (forward: 5′-ACGGGAAGCAGGTAGAGTTG-3'; reverse: 5′-CTAGGATGATGGGCACATTTGG-3′), ROCK (forward: 5′-TGGAGTACATGCCTGGTGGAGAC-3'; reverse: 5′- AGCAGCATGTTGTC AGGCTTCAC-3′), GAPDH (forward: 5′-TGACTCTACCCACGGCAAGTT CAA-3'; reverse: 5′- ACGACATACTCAGCACCAGCATCA-3′). Each reaction volume contained 5 μL 2 × SYBR Premix Ex Taq II (Takara, Dalian, China), 0.4 μL forward primer (10 μM), 0.4 μL reverse primer (10 μM), 1 μL cDNA, and ddH_2O to 10 μL. The amplification program was as follows: initial denaturation at 95 °C for 30 s; followed by 40 cycles of denaturation at 95 °C for 5 s, annealing at 55 °C for 30 s and extending at 72 °C for 30 s.

2.10. Cell stiffness measured by Young's modulus

Before the experiments, VSMCs (A7r5 or PCASMCs cells) were passaged and seeded to Petri dishes (35 mm in diameter). The seeding density was 2500 cells/cm^2. Overnight, adding ATO (0, 2, 4 and 6 μM) for 1 d. Before testing, the cells were washed with PBS three times to

remove the unattached cells and organic medium. They were finally resuspended in 1 mL PBS buffer for the experiments.

An atomic force microscope (AFM; Nanowizard II BioAFM, JPK, Germany) was used to determine the surface Young's modulus of VSMCs. The performed method was carried out as previously reported [24]. And, force curves were analyzed using JPK software.

2.11. Statistical analysis

All experiments were performed in triplicate; numerical data are expressed as mean ± standard error (SEM) and statistical significance (defined as $P < 0.05$) was determined using two-sample *t*-test using GraphPad Prism 6.

3. Results

3.1. ATO-drug eluting stent inhibits neointima formation and drives VSMCs contractile phenotype in vivo

For the direct evaluation of the role of ATO on inhibiting restenosis, three kinds of stents with bare metal stent (BMS), polymer coating-metal stent (PMS) and ATO-drug eluting stent (AES) were implanted into the carotid artery of the New Zealand male white rabbits, respectively. After 1 month (mo) of implantation, samples were observed with HE staining (Fig. 1A) and immunohistochemical (IHC) (Fig. S1) staining with α-smooth muscle actin (α-SMA). Compared with BMS and PMS, AES group had a lower neointimal hyperplasia, and the restenosis only reached to 10% (Fig. 1B). And, the thickness of neointima remained did not further aggravate post-stent for 3 mo (Fig. S2A). So, AES has excellent properties in terms of the inhibition of ISR post implantation of the stent.

To further investigate the phenotypic transformation of VSMCs in intimal hyperplasia [10,16,17], we studied the expression of contractile phenotype markers such as α-SMA and smooth muscle protein 22α (SM22α) with immunofluorescence (IF) and IHC. For IF, the fluorescence intensity of α-SMA, both of AES and BMS were significantly different from PMS group, but no difference between AES and BMS (Fig. 1C and D). While for fluorescence intensity of SM22α, AES group was stronger than BMS group at both 1 mo and 3 mo (Figs. S2B and C). From staining results of IHC, we found that compared with BMS and PMS, AES group could promote the expression of α-SMA and weaken the expression of Osteopontin, especially in the early stage of stent implantation, such as 1 week (w) (Fig. S3). Moreover, the VSMCs' morphologies were long spindle in the neointima of the AES group at 3 mo and this is similar to the mature SMCs in tunica media (Fig. 1E). In fact, the cell aspect ratio in AES group was significantly larger than that of BMS and PMS by statistics of the cell long and short axis ratio of VSMCs in neointima (Fig. 1F).

Above all, we preliminarily believe that ATO inhibits intimal hyperplasia in part by inducing VSMCs contractile phenotype formation which can promote vascular repair quickly.

3.2. ATO induces contractile VSMCs in vitro

To determine the effect of ATO on VSMCs phenotype, IF and WB were used to investigate the regulation role of ATO in the expression of VSMC-specific markers *in vitro*. The expression of contractile VSMC markers such as α-SMA (Fig. 2A and B), Calponin (Fig. S4A) as well as SM22α (Fig. S4B) were increased, but the synthetic VSMC marker Osteoponin (Fig. S4B) was weaker in ATO-treated VSMCs (A7r5, rat VSMC lines). Moreover, the cell aspect ratio was increased accordingly (Fig. 2C). And, the protein levels of both SM22α and α-SMA (Fig. 2D and E) were also increased in ATO-treated A7r5. Moreover, PCASMCs were extracted (Fig. 2F) and phenotype modulation was detected. Similarly, PCASMCs cultured to the 9th generation (cultured in high serum medium, and so considered as a synthetic phenotype VSMCs) still had the ability to transform into differentiated contractile type under ATO treatment (Figs. S5A and B).

The proliferation ability of VSMCs is also an indicator for phenotypic transformation. Thus, we determined cell viability of VSMCs (A7r5) treated ATO with different concentrations (0, 2, 4, 6, 8, 10 μM) for 1, 2 and 3 d. As shown in Fig. S6A, ATO significantly decreased the cell viability with the concentration increasing. Meanwhile, the mitochondrial membrane potential as the earliest indicator of cell apoptosis, the apoptotic number of A7r5 increased with ATO concentration dependence using flow cytometry analyzing (Fig. S6C). But, as compared to synthetic A7r5, with lower α-SMA staining (Fig. S6B), mitochondrial membrane potential showed no significant changing in contractile VSMCs (PCASMCs of 4th generation) after ATO treating (Fig. S6D). The above results indicate that ATO can inhibit cell activity and promote apoptosis in synthetic phenotype VSMCs, while has little effect on contractile phenotype VSMCs supporting the notion of ATO having different function in different phenotype of VSMC.

It has been shown that platelet-derived growth factor (PDGF) can stimulate VSMCs into synthetic phenotype and this transition can be detected at transcriptional, post-transcriptional, and epigenetic levels [25–29]. To further confirm the different regulating effect of ATO on contractile- and synthetic-phenotype VSMCs, we divided PCASMCs (the 4th generation) into two cultures: one was grown with PDGF-BB (20 ng/mL) under high serum condition to promote the synthetic phenotype; the other without PDGF under low serum conditions to keep the contractile phenotype (schematic diagram is shown in Fig. 2H). The proliferation rate of the two cells types was shown to be different based on microscopic imaging of the cells (Fig. 2G). These cells in different cultural conditions were treated with different concentration of ATO for 1 or 3 d. ATO could greatly reduce the vitality of synthetic phenotype PCASMCs by MTS assay, but contractile ones had strong tolerance to ATO, especially under 2 and 4 μM (Fig. 2I).

3.3. ATO promoting differentiation of SMCs is confirmed by RNA profiling

The aim of this part is to predict whether low-dose of ATO would has a distinguishing effect on synthetic and contractile SMCs in the future. Also, due to find the early changed genes or signaling pathways sensitive to ATO, we chose the earlier treating time of 8 h rather than other treating time such as 1 d or 3 d. To further prove that synthetic and contractile phenotypes of PCASMCs have a different response to ATO, two types of PCASMCs were treated by 2 μM ATO for 8 h, and then analyzed by RNA sequencing after extracting their total RNA (schematic diagram is shown in Fig. 3A).

The gene expression profiling was changed significantly after ATO treatment in both contractile and synthetic phenotype PCASMCs. 2916 genes were overlapped and 4477 genes were nonoverlapped in two types of PCASMCs treated by ATO (Fig. 3B). By Gene Ontology (GO) enrichment analysis (Fig. 3C), it was found that the cell processes related to VSMCs phenotypes containing cell metabolism and cell cycle were significantly changed between synthetic and contractile phenotype PCASMCs in response to ATO. Moreover, the pathways and genes were also significantly different between contractile and synthetic PCASMCs after ATO treatment (SS2 vs SH2).

The changed genes or pathways of synthetic PCASMCs with (SH2) or without (SH0) ATO treating were further analyzed, because the core question we focused on was the transformation mechanism of ATO in inhibiting the hyperplasia of synthetic SMC. The results were showed that genes expression up-regulated involves in the pathways of cell apoptosis, Hippo signal, actin cytoskeleton and vascular contraction, while the expression of genes in cell cycle, DNA replication and citrate (TCA) cycle were down-regulated (Fig. 3D). Compared with SH0 group in Fig. 3E, ATO at 2 μM significantly increased the expression of genes which could induce the cell apoptosis, inhibit cell migration, promote actin cytoskeleton assembly and transform the synthetic phenotype to contractile phenotype of PCASMCs.

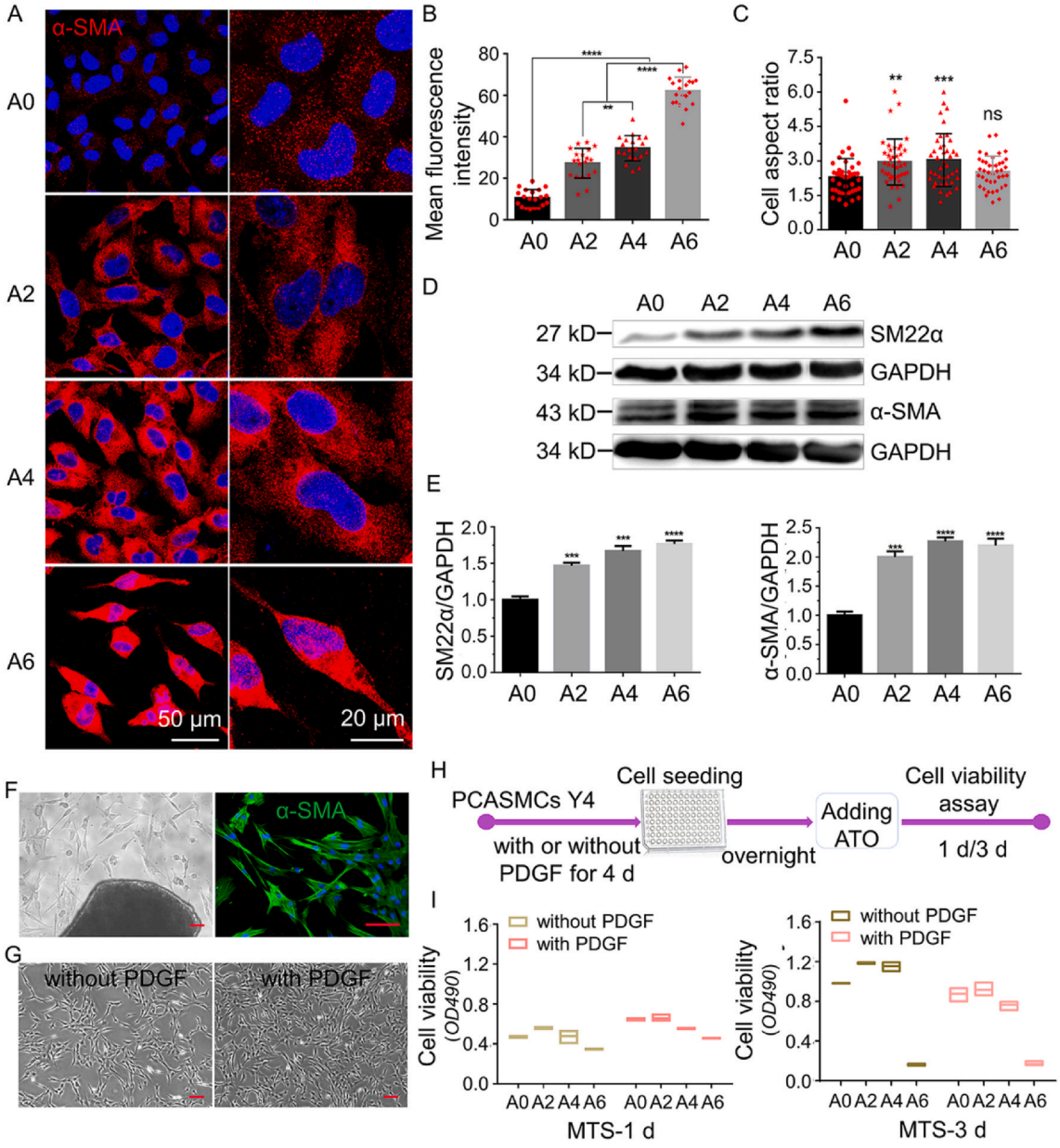

Fig. 2. *In vitro*, arsenic trioxide induces phenotype modulation, and inhibits cell viability of synthetic phenotype VSMCs. (A) α-SMA immunostaining of A7r5 with or without ATO treating for 1 d. (B) The statistical results of mean fluorescence intensity of α-SMA in (A). (C) The statistical results of cell aspect ratio (cell long/short axis ratio) of A7r5 with or without ATO treating for 1 d. (D) and (E), Protein levels of SM22α and α-SMA were determined by WB after ATO treating for 1 d. (F) The extraction and identification of primary porcine coronary artery smooth muscle cells (PCASMCs), scar bar = 100 μm. (G) The proliferation profile of PCASMCs, scar bar = 100 μm (H) The schematic diagram for the phenotype induction of PCASMCs. (I) The viability of contractile- and synthetic-phenotype PCASMCs on different concentration of ATO for 1 and 3 d. A0, A2, A4 and A6 represent 0, 2, 4 and 6 μM of ATO, respectively. "ns" means no significance, *P* values < 0.01 (**), < 0.001 (***) and < 0.0001 (****).

Further, we used qPCR of α-SMA, Calponin, RhoA, ROCK and YAP for A7r5 to validate the pathways of cell contraction, actin cytoskeleton and Hippo signal. In Fig. 3F, we found the expression of α-SMA was significantly increased treated by ATO for 1 d and 2 d, while the expression of Calponin was increased at low concentration of ATO (2 μM) no matter when 8 h, 1 d and 2 d. However, for RhoA and ROCK, low concentration of ATO (2 μM) could reduce their expression. Interestingly, the expression of YAP was reduced at 2 μM of ATO, nevertheless the reactions fluctuating with ATO concentration or treating time. Another way, the regulation of YAP activity is also subject to post-translational regulation, such as phosphorylation.

In all, ATO regulate the genes expression of cell proliferation, cell apoptosis and cell migration, actin assembly and smooth muscle contractile phenotype, which further suggests that ATO can induce the differentiation of VSMCs by regulating the phenotypic modulation. This indicates that actin cytoskeleton and Hippo signaling maybe involved in phenotypic modulation of VSMCs [30].

3.4. ATO enhances actin cytoskeleton organization and stiffness in VSMCs

Contractile phenotype VSMCs have high density and robust actin cytoskeletons [13]. As we expected, ATO obviously elevated the F-actin assembly after ATO (2 and 4 μM) treating A7r5 cells for 1 d by phalloidin staining (Fig. 4A). Furthermore, the stiffness of A7r5 cells was measured by AFM after treating with ATO. The cells treated with 2 or 4 μM ATO were much stiffer than the control by the analysis Young's

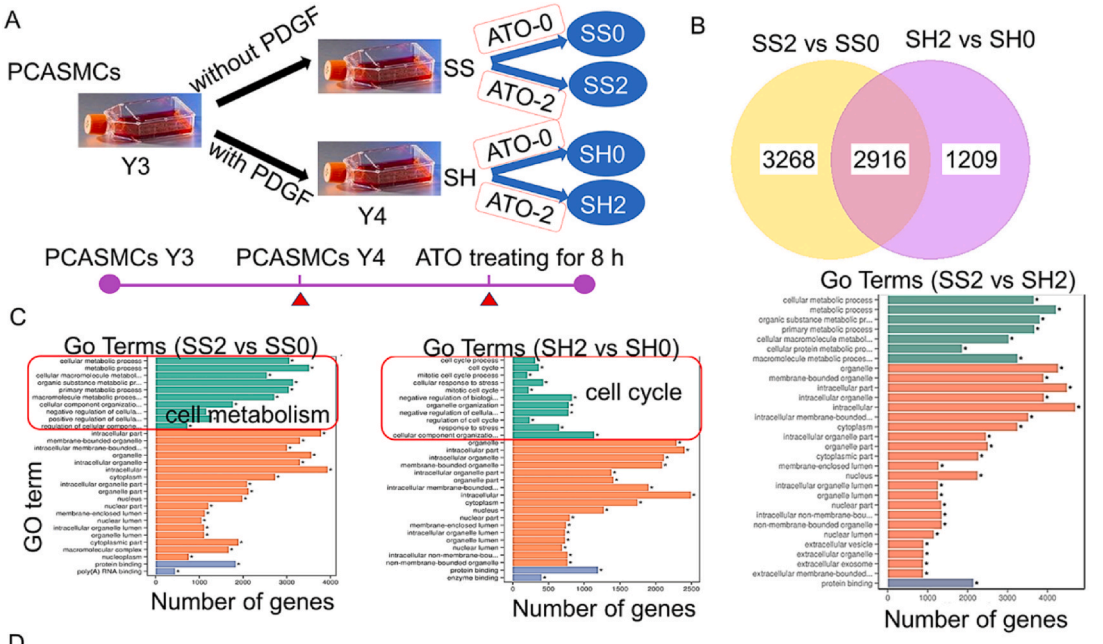

D

SH2 vs SH0	Up				Down		
Pathway	Apoptosis	Hippo signaling	Actin cytoskeleton	Vascular contraction	Cell cycle	DNA replication	TCA cycle
Gene#	18	22	30	18	55	27	13
P value	0.054	0.17	0.18	0.23	6.95E-9	2.76E-7	0.02

E

Pathway	Gene Symbol	SH2/SH0 log_2 fold change	*P* value
Apoptosis	Bcl-XL	-0.43	00015
	PIDD1	-0.54	0.00014
	CASP3	1.16	7.41E-30
	CASP9	0.54	0.00011
Cell migration	MAPK3	-0.30	0.0029
	MRLC2	-0.26	0.0048
	RhoA	-0.26	0.0013
	SRC	0.41	0.00086
	VCL	-0.46	4.03E-9
Actin cytoskeleton	ACTN1	0.31	5.13E-3
	BAIAP2	0.32	0.0035
	BPK1	0.32	0.0031
	PFN2	0.36	0.0027
	TMSB4	0.35	8.78E-6
Vascular smooth muscle contraction	ACTA2	-0.58	2.12E-14
	ACTG2	0.24	0.0032
	CNN1	0.54	6.70E-8
	FAM129A	0.59	7.32E-10
	MYLK2	2.43	2.15E-6
	PPP1R15A	1.43	8.66E-43
	PPP1R15B	0.46	7.14E-7
	TAGLN	0.23	0.0025

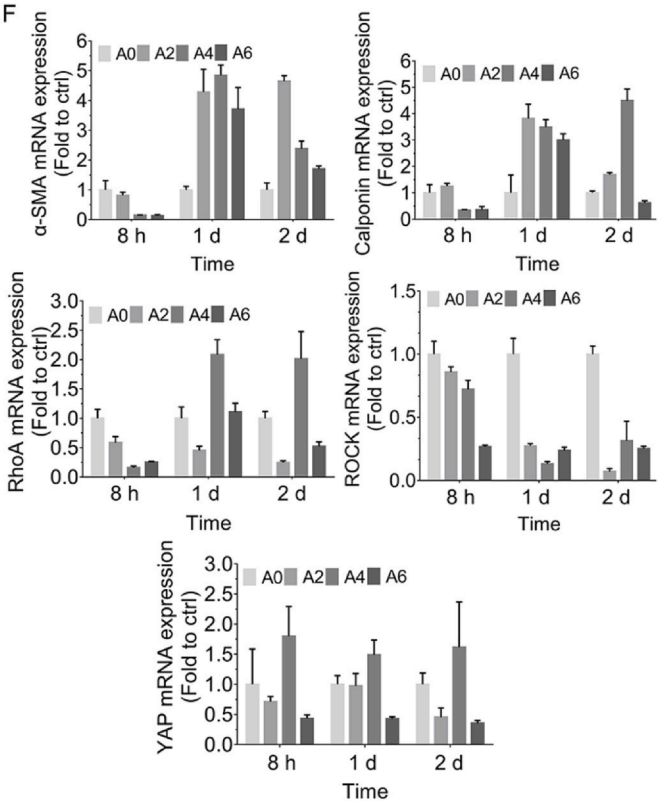

Fig. 3. RNA genome sequencing analysis of contractile and synthetic PCASMCs with or without ATO treating for 8 h, and qPCR validation of genes and signals. (A) The schematic diagram for the phenotype induction and ATO treating of PCSMCs. (B) Venn diagram. (C) Gene Ontology (GO) enrichment analysis. (D) and (E) are the statistical tables of changes in ATO treatment, related cell processes (D) and main gene expression (E) of synthetic PCASMCs (SH2 vs SH0). (F) qPCR of α-SMA, Calponin, RhoA, ROCK and YAP for A7r5. SS0: contractile PCASMCs without ATO treatment; SS2: contractile PCASMCs treated with 2 μM ATO for 8 h; SH0: synthetic PCASMCs without ATO treatment; and SH2: synthetic PCASMCs treated with 2 μM ATO for 8 h. A0, A2, A4 and A6 represent 0, 2, 4 and 6 μM of ATO, respectively.

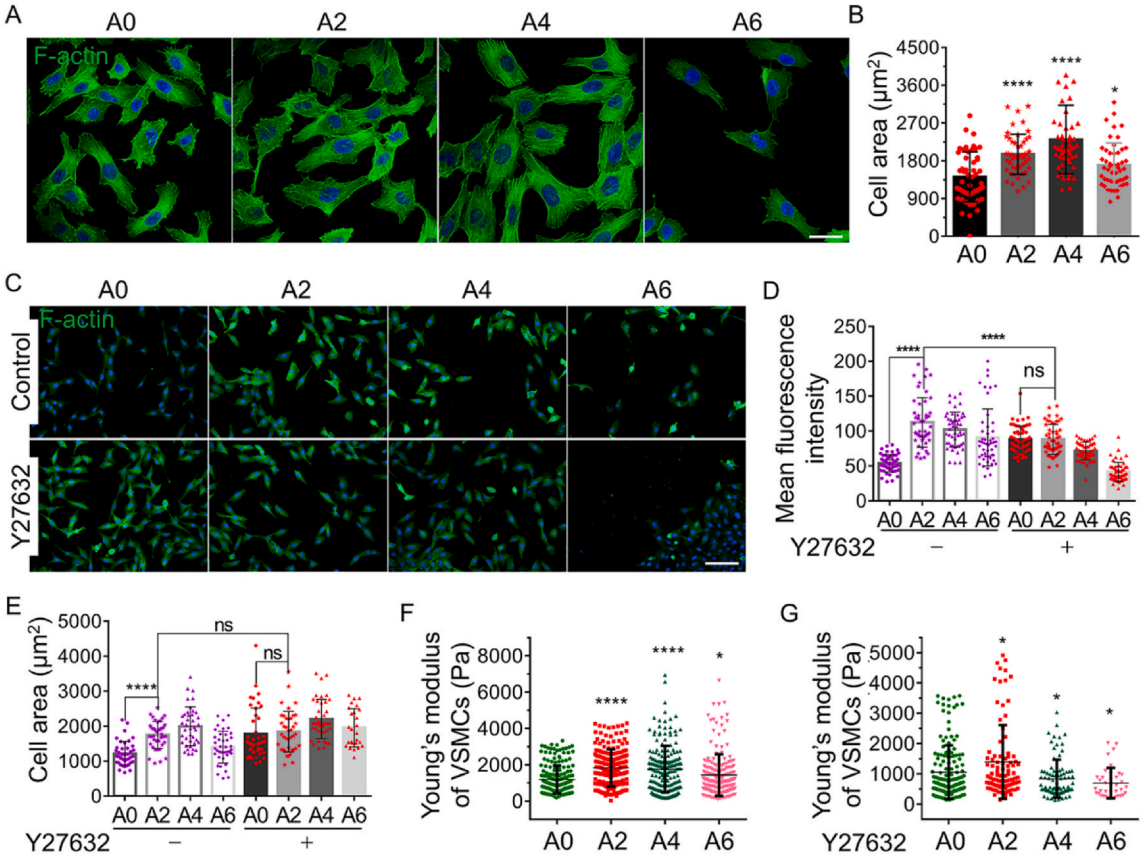

Fig. 4. ATO induces actin cytoskeleton organization and mechanical changes in VSMCs *in vitro*. (A) Immunostaining for cytoskeleton F-actin of A7r5 with or without ATO treating for 1 d, scar bar = 50 μm. (B) The statistical analysis of cell area. (C) Immunostaining for F-actin of A7r5 with or without Y27632 treating for 4 h, then treating ATO for 1 d, scar bar = 200 μm. The statistical analysis of fluorescence intensity (D) and cell area (E). (F) Young's modulus determined by atomic force microscope for A7r5 treating ATO for 1 d. (G) Young's modulus determined by atomic force microscope for A7r5 with Y27632 treating for 4 h, then treating ATO for 1 d. A0, A2, A4 and A6 represent 0, 2, 4 and 6 μM of ATO respectively; "ns" means no significance, *P* values < 0.05 (*) and < 0.0001 (****).

modulus of single cell (Fig. 4F). ATO promoted F-actin accumulation and parallelly regulated cell stiffness, and these results were also confirmed in primary PCASMCs (P9) (Figs. S5A and C).

It is well-known that actin cytoskeletal aggregation regulates the size and morphology of cells. By statistics, the cell area of VSMCs was significantly larger in both 2 and 4 μM ATO treated groups than control group (Fig. 4B). Since cytoskeletal organization could be controlled by Rho/ROCK signaling pathway [31], we examined the role of Rho/ROCK in ATO reinforcing the cytoskeleton and detected cell size and cell stiffness of VSMCs by treating cells with Y27632 (a ROCK inhibitor) for 4 h. In comparison with the untreated control group, inhibition of RhoA/Rho-associated kinase (ROCK) pathway significantly increased in actin assembly rates (Fig. 4C and D) and cell area (Fig. 4E), but changed the effect of ATO on improving the cytoskeleton assembly, cell area and cell stiffness (Fig. 4G). In a word, inhibition of ROCK activity can mask the effects of ATO on VSMCs such as F-actin aggregation, cell area and cell stiffness.

These results indicated that at moderate concentrations of ATO (2 and 4 μM) increases actin cytoskeletal aggregation and, consequently cell size, and the stiffness of VSMCs is increased. These effects appear at least in part to be mediated by which are regulated by the Rho/ROCK pathway, in that loss of this regulatory system mimics the phenotypic effect of ATO and cell lacking ROCK activity showing reduced phenotypic changes associated with ATO treatment.

3.5. ATO boots contractile phenotype formation of VSMCs by YAP pathway both in vitro and in vivo

Yes-associated protein (YAP), a highly conserved pathway regulation cell size and morphology [32], and is a central regulator of the VSMC phenotype switch and neointima formation after artery injury [33]. To confirm the function of YAP in ATO-induced VSMC phenotype switch, we discovered that ATO significantly decreased the total YAP expression and nucleic localization by IF staining (Fig. 5A). And then we performed immunostaining for YAP in cross-sections of carotid arteries post-implanting stent for 1 w. As can be seen from Fig. 5B, compared with BMS and PMS, the expression and nucleic localization of YAP in neointima were also obviously reduced in AES group. This is negatively related to the expression of smooth muscle phenotype marker α-SMA and vascular repair ability (Fig. S7). Then, we further studied the effect of ATO on the expression of YAP, SM22α and Osteopontin by using WB. Fig. 5C showed that ATO improved the expression of SM22α and reduced the expression of Osteopontin and YAP. Both *in vivo* and *in vitro*, ATO can induce contractile phenotype formation of VSMCs by inhibiting YAP activity.

The decreasing of YAP nucleus localization implies that the phosphorylated YAP may be regulated by ATO, so phosphorylated YAP at 357 (p-YAP) in A7r5 was detected by IF after treating with different concentrations of ATO for 1 d *in vitro*. Both the fluorescence intensity of p-YAP and nuclear localization were increased significantly with ATO at the concentration of 2 or 4 μM (Fig. 6A and B).

Surprisingly, p-YAP had a certain regular arrangement, which may be closely related to the arrangement of cytoskeleton from the actin and p-YAP merged image. So, we further studied the effect of ATO on the protein expression of p-YAP and SM22α by WB. Fig. 6C showed that ATO improved the phosphorylation of YAP at 357 and the expression of SM22α at the same time. And after treating with ROCK inhibitor Y27632, although the phosphorylated YAP was significantly increased,

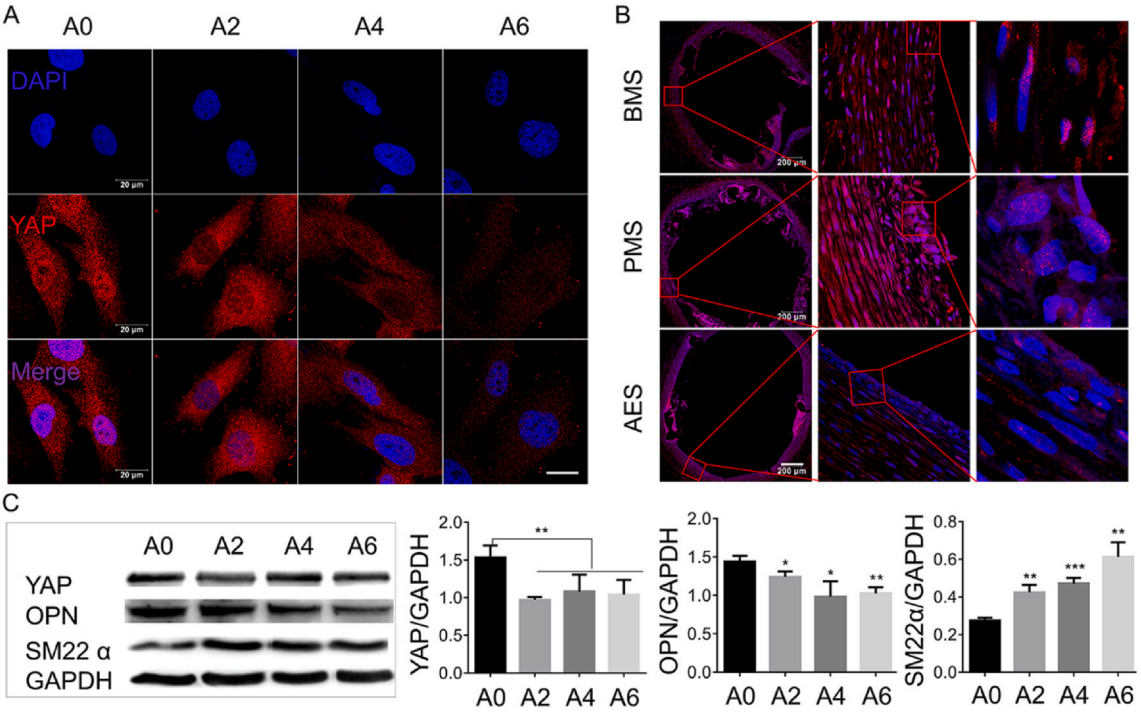

Fig. 5. ATO induces VSMCs phenotype modulation. (A) Immunostaining of YAP after ATO treating A7r5 for 1 d, scar bar = 20 μm. (B) Immunostaining for YAP in cross-sections of carotid arteries post-implanting stent for 1 week. (C) Protein expression levels of YAP, SM22α and Osteopontin (OPN) were determined by WB after ATO treating for 1 d. A0, A2, A4 and A6 represent 0, 2, 4 and 6 μM of ATO respectively; BMS (bare metal stent), PMS (polymer coating-metal stent), and AES (arsenic trioxide-drug eluting stent); *P* values < 0.05 (*), < 0.01 (**) and < 0.001 (***).

the regulation of ATO on p-YAP and SM22α was eliminated (Fig. 6C). Similarly, using YAP inhibitor verteporfin, we also found that the phosphorylated YAP and the expression of SM22α were increased after inhibiting YAP, but covered up the regulatory role of ATO both on p-YAP and SM22α (Fig. 6D). These results indicate that YAP mediates ATO driving SMC differentiation, at least in part, in a ROCK dependent manner (Fig. 6E).

4. Discussion

This study provides a novel mechanism for YAP as a mediator in ATO regulating VMSC phenotype switching and neointima formation. The main findings of our current study were as below: (i) *In vivo*, ATO-drug eluting stent (AES) can inhibit ISR, and induce VSMCs contractile phenotype modulation. (ii) *In vitro*, ATO reduces YAP activation in a ROCK dependent manner promotes VSMC contractile phenotypic modulation. Together, our findings provide a key mechanism of ATO inhibiting ISR for the first time, which means ATO modulating the VSMC phenotype partly through YAP signaling and Rho/ROCK pathway.

ATO as an anti-proliferative chemotherapy agent, was introduced into the field of DES [8,9]. Strong evidences by Gong et al. [8] and Yang et al. [34] have been presented that AES has the positive effect on inhibiting neointimal hyperplasia and ISR. We found that AES can promote vascular repairment and VSMCs mature in neointima layer while inhibiting ISR *in vivo*. In addition to inducing apoptosis, ATO was also described to induce differentiation in APL cells [35], and the effect of differentiation inducer represents a divergent approach to cancer therapy [36]. We are curious that different phenotypes of VSMCs have different responses to ATO, which would be important in maintaining the number and function of mature VSMCs, and regulating the vascular repair of activated VSMCs after vascular injury. Accordingly, our results supported that ATO have different effects on the two phenotype VSMCs. And low concentration of ATO (2 or 4 μM) reduces the cell viability and induces the cell apoptosis in synthetic phenotype VSMCs, while there is no significant effect on contractile phenotype. Other metallic stent coated with anti-proliferative drugs also the well-known treatment techniques in percutaneous coronary intervention [37–39], and function in different phenotype VSMCs maybe a common mechanism for other drugs function.

During ISR formation, VSMCs phenotypic transition toward the synthetic state is regard as an initial and central response within vascular injure repair after vascular stenting [11,12,40]. Strikingly, this study proposed the idea for the first time that ATO can induce the synthetic-to-contractile phenotype transition of VSMCs. RNA sequencing analysis and *in vitro* cell verification notes that ATO regulates the phenotypic transition of VSMC together with promoting polymerization of cytoskeletal actin and increasing the elasticity modulus. Recently, Yang et al. [12] found that miR-22 expression is downregulated in different VSMC phenotype switching models, including injured femoral arteries (*in vivo*), explanted cultured thoracic aortic tissues (*ex vivo*), and late passages of cultured VSMCs (*in vitro*). And they proved ecotropic virus integration site 1 protein homolog (EVI1) as a novel miR-22 target gene involving in VSMC phenotypic modulation. It is interesting to note that EVI1 protein can be specifically degraded by ATO. In fact, it verified our conclusion that ATO can regulate the phenotypic transformation of SMCs.

Up to now, the cell proliferation suppressed mechanisms of ATO were often explained by activating mitochondria-mediated intrinsic apoptotic signaling leading to cancer and stem cells death [7,41–43]. We discover that the contractile phenotype and stiffness of SMCs were maintained by increasing the expression of smooth muscle contractile markers (SM22α and α-SMA) and F-actin assemble, unsurprisingly, in a ROCK dependent manner.

YAP as an important factor in transduction of mechanical signals is controlled by Hippo pathway biochemically and cytoskeletal tension mechanically [44]. Previous studies reported that YAP can drive VSMC from a contractile phenotype toward a synthetic proliferative phenotype [19,45]. And we further elucidate ATO regulates VSMC phenotypic modulation by reducing YAP activation. Although we used the

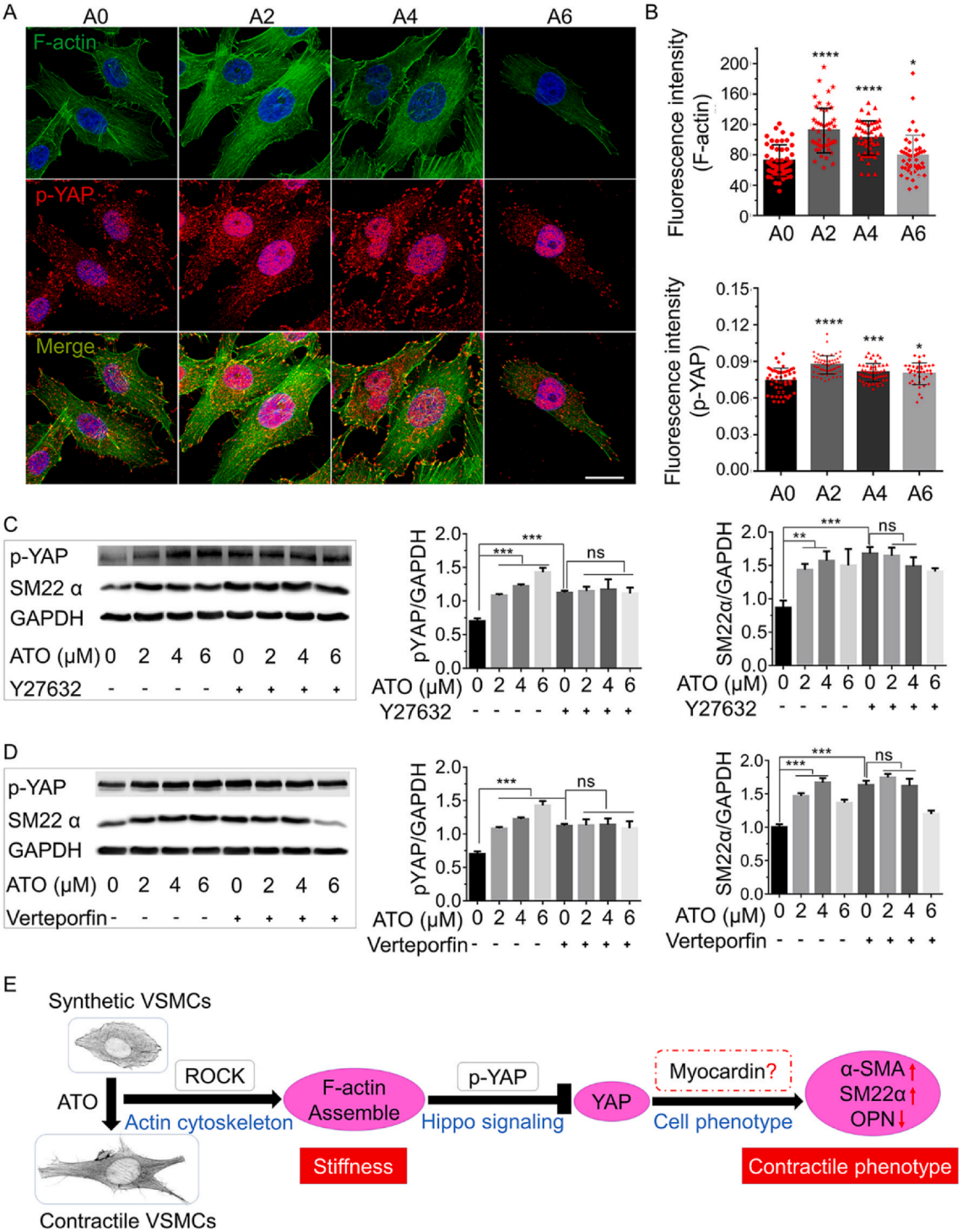

Fig. 6. The activity of YAP is associated with ATO regulating the phenotype transformation of VSMCs *in vitro*. (A) Immunofluorescence co-staining of F-actin and p-YAP after ATO treating A7r5 for 1 d, scar bar = 20 μm. (B) The fluorescence intensity of F-actin and p-YAP. (C) VSMCs (A7r5 cell lines) were treated with control or ATO for 1 d with or without ROCK inhibitor Y27632 and WB experiments for indicated the protein levels of p-YAP and SM22α were performed. (D) VSMCs (A7r5 cell lines) were treated with control or ATO for 1 d with or without YAP inactivator verteporfin and WB experiments for indicated the protein levels of p-YAP and SM22α were performed. (E) Working hypothesis which elaborates role of YAP and ROCK in ATO modulation the differentiation of VSMC. A0, A2, A4 and A6 represent 0, 2, 4 and 6 μM of ATO respectively; "ns" means no significance, *P* values $<$ 0.05 (*), $<$ 0.01 (**), $<$ 0.001 (***) and $<$ 0.001 (****).

inhibitors of YAP and ROCK to preliminary study the relationship of YAP and ROCK pathways to ATO regulating phenotypic transition of VSMCs, but the precise regulatory mechanism still needs to be further explored. The expression of YAP was significantly induced in rat balloon injury model, so blocking the function of YAP significantly up-regulated smooth muscle markers expression and decreased SMC proliferation thereby attenuating neointima formation after arterial injury [18].

5. Conclusions

These results reveal previously uncharacterized function of ATO in

regulating VSMCs synthetic-to-contractile phenotypic transition involving neointima formation, and uncover the mechanism of YAP signaling mediating the above process. We suggest a mechanism that YAP signaling as well as ROCK pathway mediate ATO driving the contractile phenotype and stiffness changes of SMCs by increasing the expression of smooth muscle contractile markers and F-actin assemble. Blocking the induction of YAP and Rho/ROCK and modulating the phenotype of SMCs would be further uncovered the clinical potential therapeutic approach of ATO for inhibiting ISR.

CRediT authorship contribution statement

Yinping Zhao: Investigation, Writing - original draft, Writing - review & editing. **Guangchao Zang:** Investigation. **Tieying Yin:** Formal analysis. **Xiaoyi Ma:** Resources. **Lifeng Zhou:** Methodology. **Lingjuan Wu:** Validation. **Richard Daniel:** Language modification and polishing. **Yunbing Wang:** Resources. **Juhui Qiu:** Conceptualization, Writing - review & editing. **Guixue Wang:** Supervision, Writing - review & editing.

Declaration of competing interest

The authors declare that they have no known competing financial interests or personal relationships that could have appeared to influence the work reported in this paper.

Acknowledgments

This study was supported in part by grants from the National Natural Science Foundation of China, China (31971242, 31701275), the National Science Foundation of Chongqing, China (cstc2020jcjy-msxmX0189), the Chongqing Research Program of Basic Research and Frontier Technology, China (CSTC2019JCYJ-ZDXM0033), Open Fund for Key Laboratory of Biorheological Science and Technology, Ministry of Education, China (CQKLBST-2019-010), Innovation Talent Project of 2020 for Chongqing Primary and secondary School, China (CY200405) and the National Key R&D Program, China (2016YFC1102305). The support from the Chongqing Engineering Laboratory in Vascular Implants, China, the Public Experiment Centre of State Bioindustrial Base (Chongqing) and the National “111 Plan”, China (B06023) are gratefully acknowledged.

Appendix A. Supplementary data

Supplementary data to this article can be found online at https://doi.org/10.1016/j.bioactmat.2020.08.018.

References

[1] S. Kozono, Y.-M. Lin, H.-S. Seo, et al., Arsenic targets Pin1 and cooperates with retinoic acid to inhibit cancer-driving pathways and tumor-initiating cells, Nat. Commun. 9 (2018) 3069.
[2] S. Waxman, K.C. Anderson, History of the development of arsenic derivatives in cancer therapy, Oncol. 6 (S2) (2001) 3–10.
[3] Z.Z. Guo, M.J. Meng, S.N. Geng, et al., The optimal dose of arsenic trioxide induced opposite efficacy in autophagy between K562 cells and their initiating cells to eradicate human myelogenous leukemia, J. Ethnopharmacol. 196 (2017) 29–38.
[4] M. Chandy, B. George, V. Mathews, et al., Treatment of children with newly diagnosed acute promyelocytic leukemia (APML) using intravenous arsenic trioxide (As_2O_3), Blood 102 (11) (2003) 620A.
[5] J. Zhu, Z. Chen, V. Lallemand-Breitenbach, et al., How acute promyelocytic leukaemia revived arsenic, Nat. Rev. Canc. 2 (9) (2002) 705–713.
[6] J.X. Liu, G.B. Zhou, S.J. Chen, et al., Arsenic compounds: revived ancient remedies in the fight against human malignancies, Curr. Opin. Chem. Biol. 16 (1–2) (2012) 92–98.
[7] P. Watcharasit, A. Thiantanawat, J. Satayavivad, GSK3 promotes arsenite-induced apoptosis via facilitation of mitochondria disruption, J. Appl. Toxicol. 28 (4) (2008) 466–474.
[8] F. Gong, X. Cheng, S. Wang, et al., Heparin-immobilized polymers as non-inflammatory and non-thrombogenic coating materials for arsenic trioxide eluting stents, Acta Biomater. 6 (2) (2010) 534–546.
[9] L. Shen, W. Yang, J.S. Yin, et al., Nine-month angiographic and two-year clinical follow-up of novel biodegradable-polymer arsenic trioxide-eluting stent versus durable-polymer sirolimus-eluting stent for coronary artery disease, Chin. Med. J. (Engl.) 128 (6) (2015) 768–773.
[10] Y. Zhao, R. Du, T. Zhou, et al., Arsenic trioxide-coated stent is an endothelium-friendly drug eluting stent, Adv. Healthc. Mater. 7 (15) (2018) 1800207.
[11] Q. Yu, W. Li, R. Jin, et al., PI3Kgamma (phosphoinositide 3-kinase gamma) regulates vascular smooth muscle cell phenotypic modulation and neointimal formation through CREB (cyclic AMP-response element binding protein)/YAP (Yes-associated protein) signaling, *Arterioscler. Thromb. Vasc. Biol.* 39 (3) (2019) e91–e105.
[12] F. Yang, Q. Chen, S. He, et al., MiR-22 is a novel mediator of vascular smooth muscle cell phenotypic modulation and neointima formation, Circulation 137 (17) (2018) 1824–1841.
[13] A. Frismantiene, E. Kyriakakis, B. Dasen, et al., Actin cytoskeleton regulates functional anchorage-migration switch during T-cadherin-induced phenotype modulation of vascular smooth muscle cells, Cell Adhes. Migrat. 12 (1) (2018) 69–85.
[14] R. Tammali, A.B. Reddy, S.K. Srivastava, et al., Inhibition of aldose reductase prevents angiogenesis in vitro and in vivo, Angiogenesis 14 (2) (2011) 209–221.
[15] U.C. Yadav, S.K. Srivastava, K.V. Ramana, Prevention of VEGF-induced growth and tube formation in human retinal endothelial cells by aldose reductase inhibition, J. Diabetes Complications 26 (5) (2012) 369–377.
[16] T. Hu, J. Yang, K. Cui, et al., Controlled slow-release drug-eluting stents for the prevention of coronary restenosis: recent progress and future prospects, ACS Appl. Mater. Interfaces 7 (22) (2015) 11695–11712.
[17] X. Wu, Y. Zhao, C. Tang, et al., Re-endothelialization study on endovascular stents seeded by endothelial cells through up- or downregulation of VEGF, ACS Appl. Mater. Interfaces 8 (11) (2016) 7578–7589.
[18] X. Wang, G. Hu, X. Gao, et al., The induction of YAP expression following arterial injury is crucial for smooth muscle phenotypic modulation and neointima formation, Arterioscler. Thromb. Vasc. Biol. 32 (11) (2012) 2662–2669.
[19] J. He, Q. Bao, M. Yan, et al., The role of Hippo/yes-associated protein signalling in vascular remodelling associated with cardiovascular disease, Br. J. Pharmacol. 175 (8) (2018) 1354–1361.
[20] Y. Du, C. Montoya, S. Orrego, et al., Topographic cues of a novel bilayered scaffold modulate dental pulp stem cells differentiation by regulating YAP signalling through cytoskeleton adjustments, Cell Prolif 52 (6) (2019) e12676.
[21] T. Christen, M.L. Bochaton-Piallat, P. Neuville, et al., Cultured porcine coronary artery smooth muscle cells: a new model with advanced differentiation, Circ. Res. 85 (1) (1999) 99–107.
[22] M. Dufresne, R. Warocquier-Clérout, Explants of porcine coronary artery in culture: a paradigm for studying the influence of heparin on vascular wall cell proliferation, Cytotechnology 37 (1) (2001) 13–22.
[23] J.K. Zeng, J.S. Guo, Z.Y. Sun, et al., Osteoblastic and anti-osteoclastic activities of strontium-substituted silicocarnotite ceramics: *In vitro* and *in vivo* studies, Bioactive Materials 5 (2020) 435–446.
[24] N. Fan, H. Jiang, Z. Ye, et al., The insertion mechanism of a living cell determined by the stress segmentation effect of the cell membrane during the tip-cell interaction, Small 14 (22) (2018) e1703868.
[25] R. Liu, Y. Jin, W.H. Tang, et al., Ten-eleven translocation-2 (TET2) is a master regulator of smooth muscle cell plasticity, Circulation 128 (18) (2013) 2047–2057.
[26] X. Guo, N. Shi, X.B. Cui, et al., Dedicator of cytokinesis 2, a novel regulator for smooth muscle phenotypic modulation and vascular remodeling, Circ. Res. 116 (10) (2015) e71–80.
[27] J. Fei, X. Cui, J. Wang, et al., ADAR1-mediated RNA editing, a novel mechanism controlling phenotypic modulation of vascular smooth muscle cells, Circ. Res. 119 (3) (2016) 463–469.
[28] N. Shi, C. Li, X. Cui, et al., Olfactomedin 2 regulates smooth muscle phenotypic modulation and vascular remodeling through mediating Runt-related transcription factor 2 binding to serum response factor, Arterioscler. *Thromb. Vasc. Biol.* 37 (3) (2017) 446–454.
[29] Y. Li, J. Huang, Z. Jiang, et al., MicroRNA-145 regulates platelet-derived growth factor-induced human aortic vascular smooth muscle cell proliferation and migration by targeting CD40, Am. J. Transl. Res. 8 (4) (2016) 1813–1825.
[30] M. Han, L. Dong, B. Zheng, et al., Smooth muscle 22 alpha maintains the differentiated phenotype of vascular smooth muscle cells by inducing filamentous actin bundling, Life Sci. 84 (13–14) (2009) 394–401.
[31] Y.T. Yeh, J. Wei, S. Thorossian, et al., MiR-145 mediates cell morphology-regulated mesenchymal stem cell differentiation to smooth muscle cells, Biomaterials 204 (2019) 59–69.
[32] R. Moreno-Vicente, D.M. Pavón, I. Martín-Padura, et al., Caveolin-1 modulates mechanotransduction responses to substrate stiffness through actin-dependent control of YAP, Cell Rep. 26 (6) (2019) 1679–1680.
[33] L. Wang, P. Qiu, J. Jiao, et al., Yes-associated protein inhibits transcription of myocardin and attenuates differentiation of vascular smooth muscle cell from cardiovascular progenitor cell lineage, Stem Cell. 35 (2) (2017) 351–361.
[34] W. Yang, J. Ge, H. Liu, et al., Arsenic trioxide eluting stent reduces neointima formation in a rabbit iliac artery injury model, Cardiovasc. Res. 72 (3) (2006) 483–493.
[35] Y.K. Zhang, C.L. Dai, C.G. Yuan, et al., Establishment and characterization of arsenic trioxide resistant KB/ATO cells, Acta Pharm. Sin. B 7 (5) (2017) 530–538.
[36] W.X. Jiang, G.Q. Cai, P.C. Hu, et al., Personalized medicine in non-small cell lung cancer: a review from a pharmacogenomics perspective, Acta Pharm. Sin. B 8 (4) (2018) 530–538.
[37] F. Liistro, G. Stankovic, C. Di Mario, et al., First clinical experience with a paclitaxel derivate-eluting polymer stent system implantation for in-stent restenosis:

immediate and long-term clinical and angiographic outcome, Circulation 105 (16) (2002) 1883–1886.
[38] M. Ali, Y. Wang, T.Y. Yin, et al., Atherosclerosis treatment with stimuli-responsive nanoagents: recent advances and future perspectives, Adv. Healthcare Mater. 8 (11) (2019) e1900036.
[39] A.J. Carter, M. Aggarwal, G.A. Kopia, et al., Long-term effects of polymer-based, slow-release, sirolimus-eluting stents in a porcine coronary model, Cardiovasc. Res. 63 (4) (2004) 617–624.
[40] J.M. Spin, L. Maegdefessel, P.S. Tsao, Vascular smooth muscle cell phenotypic plasticity: focus on chromatin remodelling, Cardiovasc. Res. 95 (2) (2012) 147–155.
[41] S. Yadav, Y. Shi, F. Wang, et al., Arsenite induces apoptosis in human mesenchymal stem cells by altering Bcl-2 family proteins and by activating intrinsic pathway, Toxicol. Appl. Pharmacol. 244 (3) (2010) 263–272.
[42] B. Cai, F. Meng, S. Zhu, et al., Arsenic trioxide induces the apoptosis in bone marrow mesenchymal stem cells by intracellular calcium signal and caspase-3 pathways, Toxicol. Lett. 193 (2) (2010) 173–178.
[43] M. Watanabe, T. Funakoshi, K. Unuma, et al., Activation of the ubiquitin-proteasome system against arsenic trioxide cardiotoxicity involves ubiquitin ligase Parkin for mitochondrial homeostasis, Toxicology 322 (2014) 43–50.
[44] M. Cantini, H. Donnelly, M.J. Dalby, et al., The plot thickens: the emerging role of matrix viscosity in cell mechanotransduction, Adv. Healthcare Mater. (2019) 1901259.
[45] F. Xu, A.S. Ahmed, X. Kang, et al., MicroRNA-15b/16 attenuates vascular neointima formation by promoting the contractile phenotype of vascular smooth muscle through targeting YAP, Arterioscler. Thromb. Vasc. Biol. 35 (10) (2015) 2145–2152.